# Kinetic Monte Carlo Study on Transient Enhanced Diffusion *Posterior to* Amorphization Process

Soon-Yeol Park, Young-Kyu Kim, and Taeyoung Won

Department of Electrical Engineering, School of Information Technology Engineering,
Inha University, Incheon, Korea 402-751
twon@hsel.inha.ac.kr

## ABSTRACT

We report our theoretical investigation on the suppression of boron diffusion in the silicon substrate *posterior to* PAI (pre-amorphization implant). We numerically investigated the defect-generating behavior of silicon atoms and the subsequent effect on the transient enhanced diffusion of boron as a new species for pre-amorphization implant (PAI). Our kinetic Monte Carlo (KMC) simulation revealed that Si-PAI produces more interstitials than the case of Ge-PAI whilst Ge-PAI makes interstitial move further up to the surface than the Si-PAI case during the annealing process, which results in the suppression of the boron transient enhanced diffusion (TED).

***Keywords***: transient enhanced diffusion, kinetic monte carlo, pre-amorphization implant.

## 1 INTRODUCTION

As devices scale down to deca-nanometer regime, the scaling scenario more stringently requires a shallow source/drain junction profile. The junction depth control is one of the key factors which alleviate the short channel effect for the deca-nanometer node technologies, especially for the high performance device. Impurity atoms which have been implanted into the silicon lattice experience various kinds of scattering events and finally stop their penetration when they lose their energy during the scattering process. It is well-known that dopant diffusion during the subsequent annealing process which is called transient enhanced diffusion (TED) deepens the junction depth[1~3]. To prevent these TED effects, pre-amorphization implant (PAI) has been considered as one of the efficient remedies in semiconductor industry. The germanium atom has been favorably employed for the PAI process because it reduces the channeling and TED diffusion of B atoms for the formation of a shallow junction. However, since the size of the germanium atom is larger than that of silicon atom, the lattice structure of the silicon substrate is considered to experience the deformation in a more severe and irregular manner. Furthermore, it has been well-known that the boron atoms experience some kind of impurity scattering. In this work, we theoretically investigated the pros and cons for the silicon PAI as an alternative to the traditional Ge-PAI process because silicon atom is the same species with the silicon substrate and the size of the silicon atom is smaller than that of the germanium, which might be expected to cause less lattice deformation.

## 2 COMPUTATIONAL DETAILS

### 2.1 Ion Implantation

In order to investigate the diffusion phenomena of boron after pre-amorphization process, we need an as-implant B profile for Si-PAI as well as Ge-PAI. In this work, we employed the BCA code for the initial as-implant dopant profile, which is based upon the Kinchin-Pease model. Kinchin-Pease model is a computationally efficient damage model based on the modified Kinchin-Pease formula proposed by Norgett et al[4]. In a simplified manner, this model accounts for damage generation, damage accumulation, defect encounters, and amorphization. The basic assumption of the Kinchin-Pease models is the nuclear energy loss which turned into point defects and the number of Frenkel pairs which is created proportionally to the nuclear energy loss. The nuclear energy loss is deposited locally and induces local defects.

### 2.2 Thermal Annealing Simulation

After implant process, we implement annealing process by using our KMC code[5,6]. In the KMC method, a physical system which consists of many possible events evolves as a series of independent event occurring. Each event has its own event rate. Event rate is calculated from the equation (1). Here, $E_b$ presents the migration energy for the barrier against the jump event of the mobile species or a binding energy for clusters. In addition, $\nu_0$ is the attempt frequency which is simply the vibration frequency of the atoms. Typically, the attempt frequency is the order of 1/100 fs. These parameters can be obtained from ab-initio calculation or experimental data.

$$v = v_0 \exp(\frac{-E_b}{K_B T}) \qquad (1)$$

Our problem is the consideration about the thermally activated events in a thermal annealing simulation after ion implantation. If the probability for the next event to occur is independent of the previous history, and the same at all times, the transition probability will be a constant which is called Poisson process. To derive the time dependence, we

can consider a single event with a uniform transition probability $r$. Let $f$ be the transition probability density which gives the probability rate at which the transition occurs at time $t$. The change of $f(t)$ over some short time interval $dt$ is proportional to $r$, $dt$ and $f$ because $f$ gives the probability density that the physical system still remains at time $t$:

$$df(t) = -rf(t)dt \qquad (2)$$

The solution of equation (2) can be easily obtained as the following wherein $r$ becomes the initial value of $f(t)$.

$$f(t) = re^{-rt}, f(0) = r \qquad (3)$$

Therefore, the simulation time is updated for($t=t+\quad t$) according to event rates as follows, because an ensemble of independent Poisson processes will behave as one large Poisson process:

$$\Delta t = -\frac{\ln u}{R}, R = \sum_{i=1}^{N} R_i \qquad (4)$$

Here, $u$ is a random number and $R$ is the total sum of all possible event rates ($R_i$). We select an event according to the event rates.

## 3 RESULTS AND DISCUSSION

Fig. 1 is a schematic diagram which illustrates the simulated B as-implant profile wherein the dotted line represents the as-implant profile without PAI, the scattered squares designate the as-implant profile with Ge-PAI, and the scattered circles represent the as-implant profile with Si-PAI. It should be further noted that the filled circles and squares represent the cases for PAI with implant energy of 20 keV while the empty circles and squares represent the cases for PAI with implant energy of 40 keV. Referring to the as-implant PAI-free B profile (dotted line) and other scattered curves (circulars and squares), we can see that the pre-amorphization process either with Ge or with Si helps to realize the shallow junction. If we look into the as-implant profiles for each type of PAI species with different implantation energies, we can see that the PAI process with 40 keV is more favorable than the case with 20 keV in terms of the depth of the as-implanted B profile. In other words, higher energy PAI seems to retard the boron channeling more effectively regardless of the species of PAI atoms. If we make comments on the species of PAI implant, the as-implant profile with Si-PAI is shallower than that with Ge-PAI.

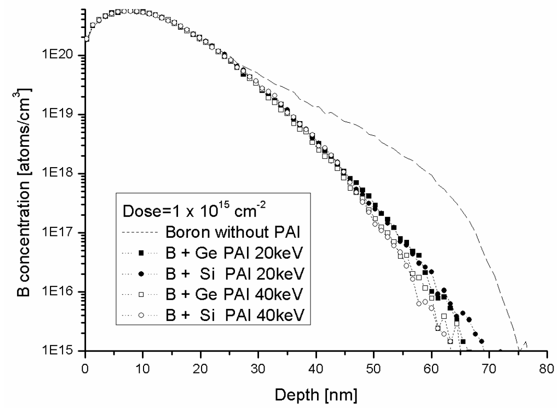


Fig. 1 Boron as-implant profiles. Boron is implanted with energy 2 keV, the dosage of 1 x $10^{15}$ /cm$^2$ after Si/Ge PAI is implemented with energy 20, 40keV and the dosage of 1 x $10^{15}$ /cm$^2$. All implantation were performed with 7 tilt angle. The dotted line represents the as-implant profile without PAI, the scattered squares designate the as-implant profile with Ge PAI, and the scattered circles represent the as-implant profile with Si-PAI. It should be further noted that the filled circles and squares represent the cases for PAI with implant energy of 20 keV while the empty circles and squares represent the cases for PAI with implant energy of 40 keV.

Fig. 2 and 3 are schematic diagrams which illustrate the simulated B profile for different annealing conditions wherein Fig. 2 corresponds to the thermal annealing for 60 seconds @ 850 ºC while Fig. 3 corresponds to the RTA for one second @ 600 ºC, respectively, for Si-PAI as well as Ge-PAI. PAI implantation was performed with a dosage of 1 x $10^{15}$ /cm$^2$ and with energy of 20 keV and 40keV, respectively. Boron implantation is performed with a dosage of 1 x $10^{15}$ /cm$^2$ and with energy of 2 keV. The solid line represents the B diffusion profile without PAI while the line with squares correspond to the cases with Ge PAI and the lines with circles represent the cases with Si PAI.

Referring to Fig. 2, we can recognize that there seems to be no significant difference in the diffusion profiles after annealing for 60 seconds. The reasons seem to be due to the fact that the boron implantation energy is relatively low when compared to the annealing time and temperature. This seems partly due to the fact that a low energy implantation induces the statistical inaccuracy and further a long duration annealing at high temperature supply enough energy for boron diffusion. In order to confirm our reasoning, we performed KMC simulation under the different annealing condition, i.e., under the RTA condition.

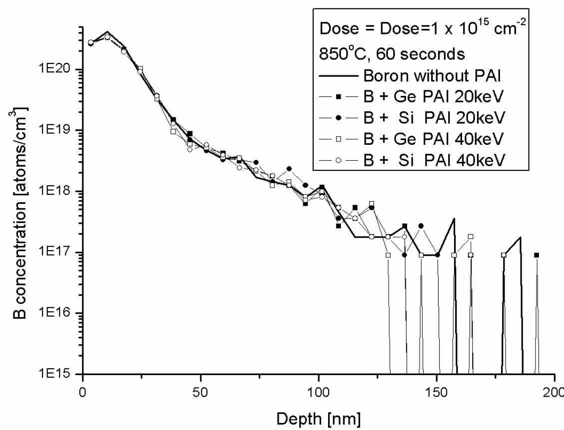


Fig. 2 Boron profile after annealing @850ºC for 60 seconds. The solid line represents the B diffusion profile without PAI while the line with squares correspond to the cases with Ge PAI and the lines with circles represent the cases with Si PAI.

Fig. 3 is a schematic diagram illustrating the diffusion profiles after annealing @600ºC for one second wherein the notations are the same as the ones used in Fig. 2. Referring to Fig.4, we can see that PAI significantly reduces the TED and PAI effect is more pronounced than the case of long time annealing. Moreover, we can see that Si-PAI with energy of 20keV is better than the other PAI cases with respect to the suppression of diffusion profiles.

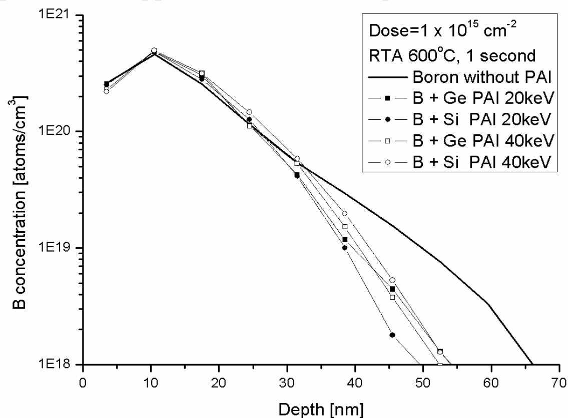


Fig. 3 Boron profile after annealing after annealing @600ºC for one second. The solid line represents the B diffusion profile without PAI while the line with squares correspond to the cases with Ge PAI and the lines with circles represent the cases with Si PAI.

In order to understand the physics behind the suppression of diffusion profiles, we investigated the defect (interstitial and vacancy) distribution with our KMC tool, which is depicted in Fig. 4 and 5. Fig. 4 is a schematic diagram which illustrates the simulated interstitial (I) distribution for Ge-PAI and Si-PAI cases under our KMC simulation. Here, the triangles represent the case with Ge PAI wherein the filled triangle represents the case with 20 keV while the empty triangle represents the case with 40 keV. Furthermore, the diamonds represent the case with Si PAI wherein the filled diamond represents the case with 20 keV while the empty diamond represents the case with 40 keV. Referring to Fig. 4, we can recognize that the interstitial distribution for the Si-PAI produces more amounts of interstitial than the Ge-PAI case near at the surface, which seems to suppress the boron diffusion more effectively than Ge-PAI[7].

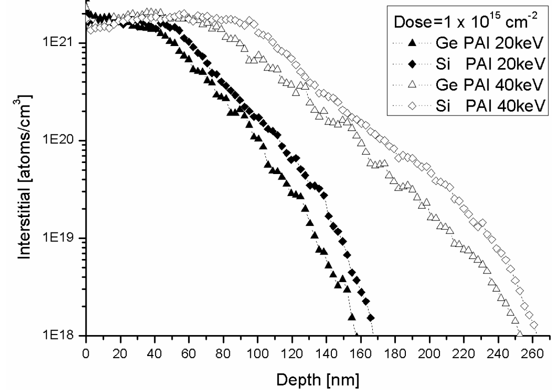


Fig. 4 A plot illustrating the simulated interstitial distributions. The triangles represent the case with Ge PAI wherein the filled triangle represents the case with 20 keV while the empty triangle represents the case with 40 keV. The diamonds represent the case with Si PAI wherein the filled diamond represents the case with 20 keV while the empty diamond represents the case with 40 keV.

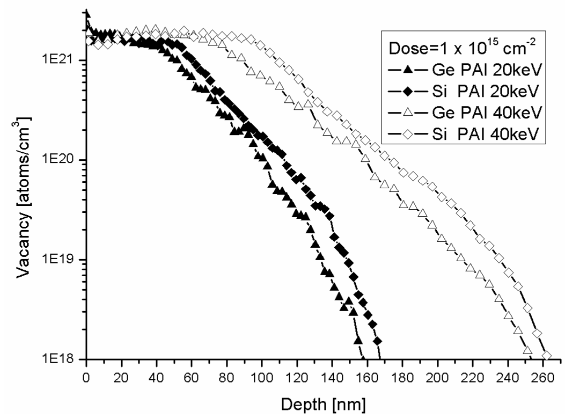


Fig. 5 A plot illustrating the simulated Vacancy distributions. The triangles represent the case with Ge PAI wherein the filled triangle represents the case with 20 keV while the empty triangle represents the case with 40 keV. The diamonds represent the case with Si PAI wherein the filled diamond represents the case with 20 keV while the empty diamond represents the case with 40 keV.

Fig. 5 is a diagram which illustrates the simulated vacancy distribution for Ge-PAI and Si-PAI cases according to our KMC simulation. Referring to Fig. 5, we can see that the vacancy profile is very similar to the interstitial profile.

Further, we simulated the change in the interstitial distribution using Si atom as well as Ge as PAI source with a dosage of 1 x $10^{15}$ /cm$^2$, and with energy of 40 keV while the boron implantation energy was 2 keV with a dosage of

1 x $10^{15}$ /cm$^2$ during the annealing process as shown in Fig. 6.

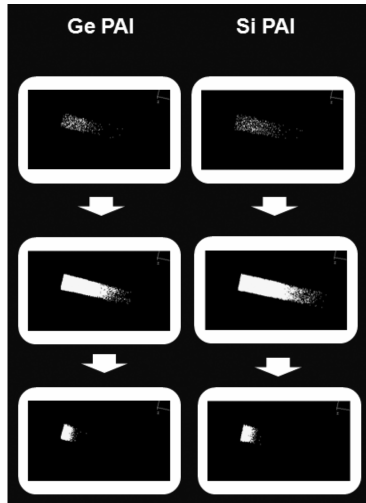


Fig. 6 Interstitial distribution changes in terms of annealing time. Finally, interstitials move toward near the surface in both PAI and both implantation energy.

Fig. 6 is a schematic diagram which illustrates the 3-dimensional interstitial distribution. In this figure, we can see that the interstitials produced by Si -PAI are formed more deeply than those of Ge PAI at the initial stage of the entire procedure while the interstitials move toward the inner depth. Finally, the interstitials are positioned near surface for both samples. The KMC simulation in Fig. 6 reveals that interstitials induced by Ge-PAI are located more near at the surface than the cases of Si-PAI. From this difference in the distribution, we can see that both PAI processes reduce the boron diffusion as the interstitials move up near to the surface.

In order to verify our KMC simulation, we compared our diffusion profiles with experimental data, which is taken from the prior published literature [8]. Referring to Fig. 7, we can see quite a good agreement between the simulated boron profile after PAI as well as the as-implant profile and the SIMS data. The numerical verification for Ge-PAI has already been conducted and reported in our in previous publication [6].

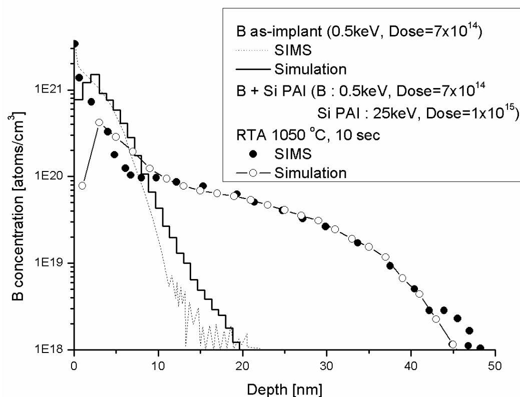


Fig. 7 KMC profile with SIMS data for as-implant B as well as the boron with Si-PAI.

## 4 CONCLUSION

In this paper, we investigated silicon atom as a new pre-amorphization implant (PAI) sources in addition to Ge atoms. Our KMC simulation revealed that the Si-PAI process produces more amount of interstitial and vacancy, which reduces the boron transient enhanced diffusion (TED). We compared the effects of Si-PAI with those of Ge-PAI under the same annealing condition. From the KMC investigation of the interstitial distribution, we found that Si-PAI produces more interstitials than the case of Ge-PAI while Ge-PAI makes interstitial move further to the surface than the Si-PAI case during the annealing process.

## ACKNOWLEDGMENT


This research was supported by the Ministry of Knowledge and Economy, Korea, under the ITRC (Information Technology Research Center) support program supervised by the IITA (Institute of Information Technology Advancement) (IITA-2008-C109008010030).


## REFERENCES


[1] P.M. Fahey, P. B. Griffin, and J. D. Plummer, Rev Mod. Phys. 61, 289 (1989).

[2] P. A. Stolk, H-J. Gossmann, D. J. Eanglesham, D. C. Jacobson, C. S. Rafferty, G. H. Gilmer, M. jaraiz, J. M. poate, H. S. Luftman, and T. E. Haynes, J. Appl. Phys. 81, 6031 (1977).

[3] A. Agarwal, H-J. Gossmann, D. J. Eaglesham, S. B. herner, A. T, Fiory, and T. E. Haynes, J. Appl. Phys. 81, 6031 (1997).4. P.M. Fahey, P.B. Griffin, and J. D. Plummer, Rev Mod. Phys. 61, 289 (1998).

[4] M. J. Norgett. M. T. Robinson, and I. M. Torrens, Nucl. Eng. Des., 33, 50, (1975).

[5] Jae-Hyun Yoo, Chi-Ok Hwang, Byeong-Jun Kim, and Taeyoung Won, Simulation of Semiconductor Processes and Devices 2005, pp.71-74, (2005).

[6] Joong-sik Kim, Taeyoung Won, Microelectronic Engineering, 84, 1556, (2007).

[7] A. Ural, P. B. Griffin, and J. D. Plummer, J. Appl. Phys. 85, 6440 (1999).

[8] B. J. Pawlak, T. Janssens, B. Brijs, and W. Vandervorst, E. J. H. Collart, S. B. Felch and N.E.B. Cowern, Appl. Phys. Letters 89, 062110 (2006).